DOI: 10.61782/fa.2025.0442

FORUM ACUSTICUM
EURONOISE 2025

IMAGING-BASED SAXOPHONE REED MODELLING

Diego Tonetti[1*] **Edoardo Piana**[1]

[1] Department of Mechanical Engineering, University of Brescia, Italy

ABSTRACT

Accurate sound synthesis of reed instruments based on physical models is of primary importance in the development and prediction of the sound produced by such devices. Since the sound is produced by reed oscillation, correct modelling of this part is mandatory. Several attempts have been explored in literature both by direct and inverse modelling. Here an imaging-based approach for characterising the reed dynamic behaviour is presented, using a high-speed camera and a Digital Image Correlation technique that allows the measurement of the reed vibrations under exponential sine sweeps pressure excitation signals. The transfer function between the reed and the driving pressure is estimated at different jaw forces using an artificial lip. This approach allows for direct modelling of the reed as a single-degree-of-freedom oscillator that can be implemented in sound synthesis.

Keywords: *reed, computer vision, high-speed camera, saxophone*

1. INTRODUCTION

The saxophone reed is responsible for the sound the instrument generates since its vibration generates a pressure variation over time that the instrument's body amplifies. Its oscillating frequency differs from its natural frequency, and it is imposed by the resonance frequency of the instrument in a feedback mechanism. Modelling the instrument-reed interaction has been first studied for a clarinet-like instrument (such as the saxophone) in [1], where the reed is assumed to behave as a single-degree-of-freedom oscillator, with the oscillations forced by the pressure difference across its surface. The same assumption on the reed dynamics is the most common approach in literature and is used by many authors [2–6]. Others simplify the reed model by assuming that the resonance frequency is much higher than the instrument's one, leading to a quasi-static model of the reed where the displacement is directly proportional to the pressure difference [7, 8]. This simplification is no longer valid as the instrument resonance frequency gets closer to the reed resonance frequency, thus, it is of mandatory importance to estimate its frequency response. Here, the reed transfer function that relates the reed motion to the acoustic pressure is estimated with a high-speed camera and a microphone. Digital Image Correlation is used as an image tracking algorithm to measure the reed displacement. Lip influence is considered, and the transfer function is measured at different biting forces. At last, least-squares optimization is used to fit a numerical model of the reed with experimental data, retrieving the reed stiffness, resonance frequency and damping for each lip force.

2. MATHERIALS AND METHODS

Following the acousto-mechanical modelling of the reed from the literature, the transfer function defined in Eq. (1) that relates the reed displacement $y(t)$ with the acoustic pressure $p(t)$ is estimated to retrieve the resonance frequency ω_r, the stiffness k_r and the damping ξ of the reed.

$$\ddot{y}(t) + 2\xi\omega_r\dot{y}(t) + \omega_r^2 y(t) = \frac{\omega_r^2}{k_r}p(t) \qquad (1)$$

A synthetic reed (Legere 3 tenor saxophone reed) is measured with a high-speed camera Mikrotron Cube7 and

*Corresponding author: diego.tonetti@unibs.it.

a Bruel & Kjaer 4170 microphone inserted in the mouthpiece via a lateral hole placed 2 mm away from the reed tip. The microphone pressure is acquired with a Bruel & Kjaer Pulse acquisition system. Calibration of the image system is performed with a calibration sheet, which is used to compute the pixel-to-millimeter ratio, while the microphone is calibrated with a pistonphone Bruel & Kjaer type 4228. The chosen reed is made of a synthetic material, allowing us to discard the humidity's effect on the reed's flexibility, leading to more constrained boundary conditions. The reed is mounted on a saxophone mouthpiece, with a speaker connected to the mouthpiece through the hole where the saxophone neck is usually fitted. The effect of the player's lip biting on the reed is simulated with a soft foam of 10mm by 20mm and 5mm thick, with a hanging mass that determines the jaw force applied. The mass is varied from 0g to 1000g with steps of 250g, to simulate different biting forces on the reed. The 0g condition is achieved by removing the artificial lip, which means that the reed is simply clamped to the mouthpiece via the ligature. A constant light source is placed behind the reed, acting as a bright background in the recorded images and allowing for higher contrast in images, which is mandatory for image analysis. The experimental setup is schematized in Figure 1.

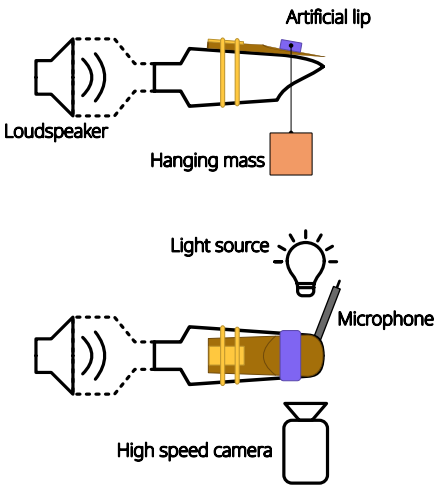

Figure 1. Scheamtic lateral and top view of the experimental setup.

The chosen signal is an exponential sine sweep generated with the plugin Aurora for Audacity [9], which also computes the inverse filter that will be used to remove all the harmonic distortions of the measured signals, allowing the retrieval of the linear response of the reed. For a signal $s(t)$, this is achieved by computing the convolution between the signal and the inverse filter as in Eq. (2):

$$r(t) = s(t) * x^{-1}(t) \tag{2}$$

where $x^{-1}(t)$ is the inverse filter of the exponential sine sweep $x(t)$. Looking at the time series of the convolution result $r(t)$, a series of peaks that correspond to the impulse responses of each harmonic is visible [10]. The linear response is the last impulse response visible in the series and can be isolated by taking a time window around it. An example of the convolution result is presented in Figure 2.

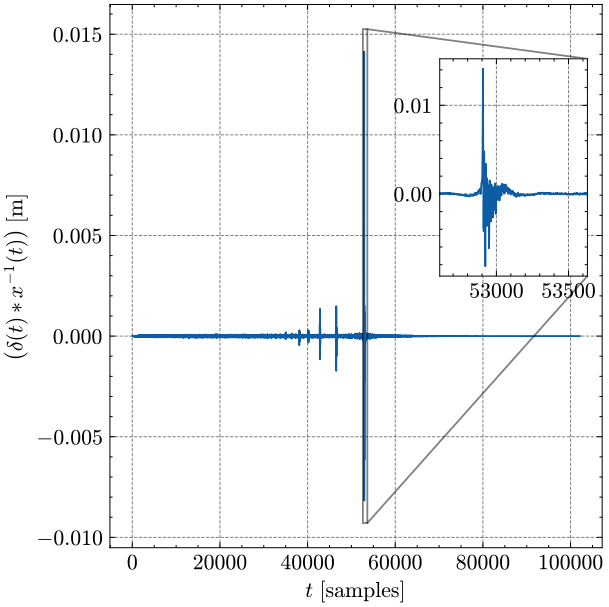

Figure 2. Convolution result of the measured displacement with a load of 0 g. A zoom is performed on the linear response.

Once the linear impulse responses of the pressure and displacement are retrieved, the measured transfer function of the reed $H_m(f)$ is evaluated in Eq. (3) as the ratio of the FFTs of the windowed impulse responses of the displacement $\delta'(t)$ and the pressure $p'(t)$.

$$H_m(f) = \frac{\mathcal{F}(\delta'(t))}{\mathcal{F}(p'(t))} \tag{3}$$

Performing the Laplace transform of Eq. (1) using the operator $s = j\omega = 2j\pi f$ leads to Eq. (4).

$$H(s) = \frac{Y(s)}{P(s)} = \frac{1}{k_r} \frac{\omega_r^2}{s^2 + 2\xi\omega_r s + \omega_r^2} \quad (4)$$

The measured transfer function can then be used to estimate the resonance frequency ω_r, the damping ξ and the elastic coefficient k_r of Eq. (1) by fitting the analytical transfer function $H(s)$ with the experimental transfer function $H_m(f)$. This can be done with least-squares optimization that aims at finding ω_r, ξ and k_r as in Eq. (5).

$$(\omega_r, \xi, k_r) = \arg\min_{\mathbf{b}} \| |H(f, \mathbf{b})| - |H_m(f)| \|, \quad \forall f \quad (5)$$

2.1 Image tracking

Tracking the reed's movement can be trivial, but the choice of image-tracking algorithm is crucial for the correctness of the obtained results. Digital image correlation (DIC) [11] is used here to track the movement of the reed; this procedure allows for computing the image shift between two different frames by computing the cross-correlation function between them, similar to the technique used to calculate the time-lag between two audio signals. The technique can be easily applied due to the image setup constraint, as it is possible to isolate the reed movement entirely from the surrounding ambient, as can be observed in Figure 3, where the only moving object is the reed.

Figure 3. Reed tip acquired by the camera.

The cross-correlation between two images can be computed efficiently with the discrete Fourier transform (DFT) as

$$r = \mathcal{F}^{-1} \left(G_a \circ G_b^* \right) \quad (6)$$

where $\circ$ is the element-wise multiplication of the DFT G_a and G_b of the image I_a at time t and the reference image I_b. The displacement is then equal to the position of the maximum correlation coefficient and can be retrieved as

$$(\Delta x, \Delta y) = \arg\max_{(i,j)}(r) \quad (7)$$

This approach is limited to discrete displacements of 1 pixel, while sub-pixel precision is required due to the small movements of the reed. A straightforward solution is to interpolate the cross-correlation function and find the new maximum given by that interpolation [12], thus achieving sub-pixel accuracy. Here, a 3rd order interpolation is used from the Python [13] library Scipy [14] by performing a zoom with an enlargement factor $Z = 10$, which leads to a sub-pixel accuracy of 0.1 pixel. To save computational costs, interpolation is performed on a small window around the pixel-level peak. The overall displacement due to the pixel displacement plus the sub-pixel displacement is then given by Eq. (8) as

$$(\Delta x, \Delta y) = \arg\max_{(i,j)}(r) + \frac{1}{Z} \arg\max_{(i,j)}(r') \quad (8)$$

where r' is the interpolated cross-correlation. To avoid problems at the borders that could cause aliasing, the images are multiplied by a two-dimensional Hann window. Also, contrast is enhanced via histogram stretching and noise is reduced with a Gaussian blur using OpenCV [15]. The algorithm steps are reported here:

1. Compute the FFT of the reference image multiplied by the Hann window.
2. Compute the FFT of the image at time instant t.
3. Compute the cross-correlation with Eq. (6).
4. Find the pixel-precision displacement with equation 7.
5. Crop the cross-correlation around the peak found in the previous step.
6. Interpolate the cross-correlation and retrieve the sub-pixel displacement again with 7.
7. Scale the sub-pixel displacement by the zoom factor and add it to the pixel-level displacement.

3. RESULTS

All the measurements are performed with a sine sweep that goes from 50 Hz up to 5 kHz with a duration of 5 s, and the sampling frequency is chosen equal to the framerate of the camera, i.e. 10 kHz. The window used around the peak is of 1024 samples, with a sampling frequency of 10 kHz, thus leading to a frequency resolution of 9.77 Hz. The experimental transfer function of the reed measured for all the lip loads is presented in Figure 4, where both the amplitude and the phase are shown.

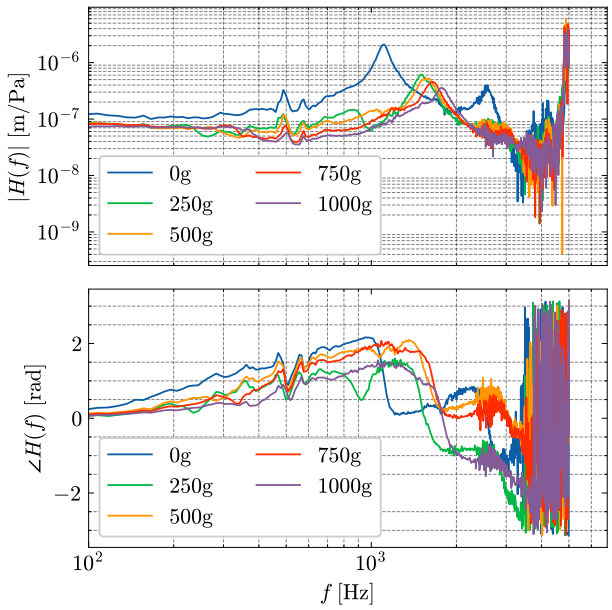

Figure 4. Reed measured transfer functions at different loads.

Comparisons between the measured and least-squares transfer functions are reported for various lip loads in Figure 5. Only the modules of the transfer functions are considered during the least-squares method, as the phase at low frequency presents a drift that makes the single DOF oscillator unfit. Following the control theory of Linear Time Invariant systems in the Laplace domain, the phase shift could be modelled by adding a zero (i.e. a derivative term) at low frequency in the transfer function of Eq.(4), which would increase the phase by 90 deg in agreement with the results, but it would also increase the module by 20 dB/dec which is not visible in the measures. Thus, following the literature, Eq. (4) is considered valid, the phase is discarded, and only the module is used for fitting the transfer function with experimental data. The data is fitted on the frequencies that range from 50 Hz to 2500 Hz to avoid noise at high frequency and at the low frequencies where the reed isn't excited by the ESS.

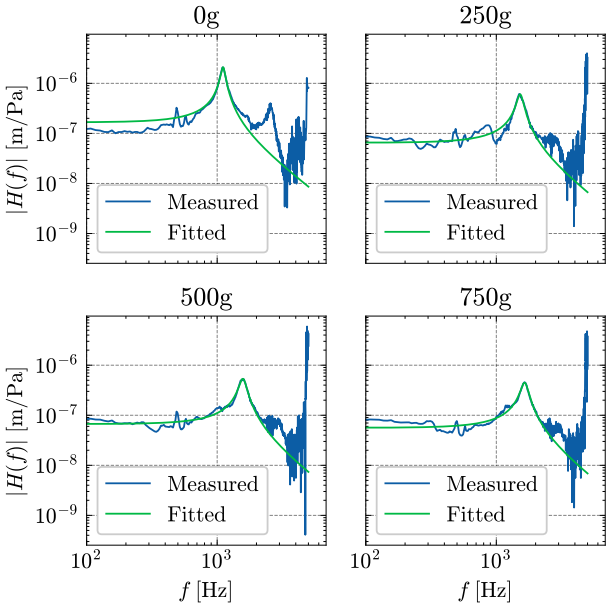

Figure 5. Measured and least-squares optimization results for 4 different lip loads.

The fitted transfer functions are reported in Figure 6, while the estimated coefficients derived from the least-squares optimization are summarized in Table 1.

load [g]	k_r [Pa/m]	ω_r [rad/s]	ξ [1]
0	6.01×10^6	6.97×10^3	3.95×10^{-2}
250	1.54×10^7	9.59×10^3	5.40×10^{-2}
500	1.50×10^7	9.92×10^3	6.24×10^{-2}
750	1.78×10^7	1.04×10^4	6.27×10^{-2}
1000	1.95×10^7	1.12×10^4	7.71×10^{-2}

Table 1. Caption

4. DISCUSSIONS

From the measured reed transfer function with no lip force applied, two resonance peaks are visible, one at 1104 Hz and one at 2549 Hz. The presence of two resonances is not visible when a lip load is applied; this could be a limitation

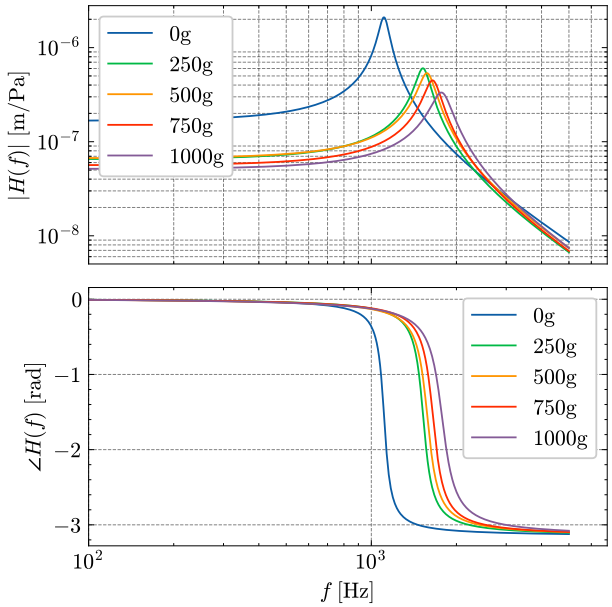

Figure 6. Fitted transfer function of the reeds at all lip loads.

of the experimental setup used, as it presents considerable noise above 3 kHz. A better signal-to-noise ratio can be achieved using a brighter light source, enhancing the image contrast. The reed's first resonance in the absence of lip influence is in agreement with the one measured in [16] for a tenor saxophone cane reed. The first resonance peak is shifted up in frequency as the lip load increases, which is in contrast with the measurements obtained in [5]. This behaviour of the reed increasing its resonance frequency is indirectly observed in [17] and is well known by players, where higher biting forces increase the pitch of the note. In [17], this is justified by stating that the reed is bent against the mouthpiece, thus shortening the reed portion that is allowed to vibrate. The measured resonance frequency and reed stiffness are close to the results obtained by inverse modelling of a clarinet reed in [6], and the reed stiffness is also comparable with the results found for a quasi-static clarinet reed [8]. Significant discrepancies are found with the resonance frequency, stiffness and damping with [18], where inverse modeling similar to [6] was performed on a tenor saxophone reed.

5. CONCLUSIONS

The transfer function of a reed was directly measured at different lip forces via a high-speed camera and Digital Image Correlation. This technique allowed non-contact measures of the reed displacement, representing an alternative to Laser Doppler Vibrometry. The performed measurements were compared with the literature, finding mixed results. These discrepancies could be due to the experimental setups, artificial lips and reed materials. The resonance frequency of the reed is found to be around 20 times greater than the instrument's lowest resonance frequency, while about only 3 times larger than the highest. A quasi-static model of the reed could thus be insufficient to model the reed as the note of interest moves up along the saxophone register.

6. ACKNOWLEDGMENTS

The authors thank Prof. Pietro Poesio and Prof. Davide Picchi (Fisica Tecnica Industriale Laboratory, the University of Brescia) and Dr. Simone Pasinetti (Misure Meccaniche e Termiche Laboratory, the University of Brescia) for lending the high-speed camera and the lens, respectively.

7. REFERENCES

[1] R. T. Schumacher, "Ab initio calculations of the oscillations of a clarinet," *The Journal of the Acoustical Society of America*, vol. 65, pp. S73–S73, 08 2005.

[2] A. Chaigne and J. Kergomard, *Acoustics of Musical Instruments*. Modern Acoustics and Signal Processing, Springer New York.

[3] S. Wang, E. Maestre, and G. Scavone, "Acoustical modeling of the saxophone mouthpiece as a transfer matrix," *The Journal of the Acoustical Society of America*, vol. 149, pp. 1901–1912, 03 2021.

[4] S. Bilbao, "Direct Simulation of Reed Wind Instruments," *Computer Music Journal*, vol. 33, pp. 43–55, Dec. 2009.

[5] J. Dalmont, B. Gazengel, J. Gilbert, and J. Kergomard, "Some aspects of tuning and clean intonation in reed instruments," *Applied Acoustics*, vol. 46, no. 1, pp. 19–60, 1995. Musical Instrument Acoustics.

[6] V. Chatziioannou and M. Van Walstijn, "Estimation of clarinet reed parameters by inverse modelling," *Acta*

Acustica united with Acustica, vol. 98, pp. 629–639, 07 2012.

[7] J. Gilbert, S. Maugeais, and C. Vergez, "Minimal blowing pressure allowing periodic oscillations in a simplified reed musical instrument model: Bouasse-Benade prescription assessed through numerical continuation," *Acta Acustica*, vol. 4, no. 6, p. 27, 2020.

[8] J.-P. Dalmont, J. Gilbert, and S. Ollivier, "Nonlinear characteristics of single-reed instruments: Quasistatic volume flow and reed opening measurements," *The Journal of the Acoustical Society of America*, vol. 114, pp. 2253–2262, 10 2003.

[9] Angelo Farina, "Aurora for audacity."

[10] farina angelo, "advancements in impulse response measurements by sine sweeps," *journal of the audio engineering society*, may 2007.

[11] P. E. Anuta, "Spatial Registration of Multispectral and Multitemporal Digital Imagery Using Fast Fourier Transform Techniques," *IEEE Transactions on Geoscience Electronics*, vol. 8, pp. 353–368, Oct. 1970.

[12] B. Xiong, Q. Zhang, and V. Baltazart, "On Quadratic Interpolation of Image Cross-Correlation for Subpixel Motion Extraction," *Sensors*, vol. 22, p. 1274, Feb. 2022.

[13] G. Van Rossum and F. L. Drake, *Python 3 Reference Manual*. Scotts Valley, CA: CreateSpace, 2009.

[14] P. Virtanen, R. Gommers, T. E. Oliphant, M. Haberland, T. Reddy, D. Cournapeau, E. Burovski, P. Peterson, W. Weckesser, J. Bright, S. J. van der Walt, M. Brett, J. Wilson, K. J. Millman, N. Mayorov, A. R. J. Nelson, E. Jones, R. Kern, E. Larson, C. J. Carey, İ. Polat, Y. Feng, E. W. Moore, J. VanderPlas, D. Laxalde, J. Perktold, R. Cimrman, I. Henriksen, E. A. Quintero, C. R. Harris, A. M. Archibald, A. H. Ribeiro, F. Pedregosa, P. van Mulbregt, and SciPy 1.0 Contributors, "SciPy 1.0: Fundamental Algorithms for Scientific Computing in Python," *Nature Methods*, vol. 17, pp. 261–272, 2020.

[15] G. Bradski, "The OpenCV Library," *Dr. Dobb's Journal of Software Tools*, 2000.

[16] B. Gazengel and J.-P. Dalmont, "Mechanical response characterization of saxophone reeds," in *Proceedings of "Forum Acusticum"*, (Aalborg, Denmark), p. 000124, June 2011.

[17] A. Almeida, D. George, J. Smith, and J. Wolfe, "The clarinet: How blowing pressure, lip force, lip position and reed "hardness" affect pitch, sound level, and spectrum," *The Journal of the Acoustical Society of America*, vol. 134, pp. 2247–2255, Sept. 2013.

[18] A. Muñoz Arancón, B. Gazengel, J.-P. Dalmont, and E. Conan, "Estimation of saxophone reed parameters during playing," *The Journal of the Acoustical Society of America*, vol. 139, pp. 2754–2765, 05 2016.